

Influence of the interaction potential and of the temperature on the thermodiffusion (Soret) coefficient in a model system

Cite as: J. Chem. Phys. **128**, 054507 (2008); <https://doi.org/10.1063/1.2830716>

Submitted: 29 August 2007 . Accepted: 10 December 2007 . Published Online: 07 February 2008

Erminia Leonardi, Bruno D'Aguzzo, and Celestino Angeli



View Online



Export Citation

ARTICLES YOU MAY BE INTERESTED IN

[Computing the Soret coefficient in aqueous mixtures using boundary driven nonequilibrium molecular dynamics](#)

The Journal of Chemical Physics **122**, 114503 (2005); <https://doi.org/10.1063/1.1863872>

[Soret and mass diffusion measurements and molecular dynamics simulations of n-pentane-n-decane mixtures](#)

The Journal of Chemical Physics **116**, 3718 (2002); <https://doi.org/10.1063/1.1436473>

[A comprehensive study of diffusion, thermodiffusion, and Soret coefficients of water-isopropanol mixtures](#)

The Journal of Chemical Physics **136**, 244512 (2012); <https://doi.org/10.1063/1.4730306>

PHYSICS TODAY
WHITEPAPERS

ADVANCED LIGHT CURE ADHESIVES

Take a closer look at what these environmentally friendly adhesive systems can do

READ NOW

PRESENTED BY
MASTERBOND
ADHESIVES | SEALANTS | COATINGS



Influence of the interaction potential and of the temperature on the thermodiffusion (Soret) coefficient in a model system^{a)}

Erminia Leonardi,^{1,b)} Bruno D'Aguzzo,¹ and Celestino Angeli²

¹CRS4, Center for Advanced Studies, Research and Development in Sardinia, Parco Scientifico e Tecnologico, POLARIS, Edificio 1, 09010 Pula, Italy

²Dipartimento di Chimica, Università di Ferrara, Via Borsari 46, I-44100 Ferrara, Italy

(Received 29 August 2007; accepted 10 December 2007; published online 7 February 2008)

In this paper the thermodiffusive behavior of an equimolar binary mixture subject to repulsive potentials of the form $(\sigma/r)^n$ is investigated by using nonequilibrium molecular dynamics (NEMD) and the thermodiffusion (Soret) coefficient, S_T , is computed in a wide range of temperatures. With the aim to contribute to the study of the dependence of the Soret coefficient on the interaction potential, the exponent n of the potential is varied from 1 to 12, that is from a pseudocoulombian to a pseudohard-sphere interaction. The steady state equation is integrated for the composition function under reasonable assumptions and it is shown that in some cases the request for it to be linear cannot be satisfied. For this reason nonlinear functions are used to fit the NEMD composition data. The simulations indicate a negligible dependence of S_T on the composition (in the composition range here considered) while the dependence on the temperature is more marked. The computed values of S_T as a function of the temperature are fitted with analytical functions. It is found that with $n \geq 3$ (medium and short range interaction) the model system behaves like a dilute gas mixture with the Soret coefficient varying with the temperature almost like $1/T$. In the case of $n=1$ (long range interaction), S_T has a more complex dependence on T : in particular it shows a change of sign. The analytical fitting functions, $S_T(T)$, are used in the integrated steady state equation thus obtaining the steady state composition profile and its comparison with the NEMD results indicates the grounding of the approach here proposed. © 2008 American Institute of Physics. [DOI: 10.1063/1.2830716]

I. INTRODUCTION

Thermodiffusion, also called the Ludwig–Soret effect, describes the coupling between a temperature gradient and an induced resulting mass flux in a multicomponent system. It is a nonequilibrium effect and is rationalized in the nonequilibrium thermodynamics, where it is a typical example of a crossed effect (a mass flux depends on a heat flux). At the steady state two opposing flows, the one due to ordinary diffusion and the one due to thermal diffusion, must exactly balance out. In order to reach a steady state it is therefore necessary to have a concentration gradient of the various species composing the system and the amplitude and sign of the separation are characterized by the so-called Soret coefficient, S_T .

The intriguing aspect of thermodiffusion is that, although Ludwig and Soret discovered the effect in the 19th century,^{1,2} “it remains the only hydrodynamic transport mechanism that lacks a simple physical explanation”³ or, more recently, “there is so far no molecular understanding of thermodiffusion in liquids.”⁴ On the other hand, the effect is relevant in many technical applications as, for instance, polymer characterization,⁵ analysis of petrol reservoir,⁶ characterization and accumulation of uranium,⁷ flame structures of burning methane and hydrogen,^{8,9} study of charged

micelles¹⁰ and colloids,¹¹ magnetic particles in ferrofluids,¹² in thermal field flow fractionation,¹³ and in energy storage in solar ponds.¹⁴ Recently, the Soret effect has been found to be relevant also in DNA and protein biotechnology.^{15–17} In particular Braun and Libchaber¹⁶ have proposed that core processes of life evolution can be driven by thermodiffusion, especially if it is coupled with convective motions.

Therefore, an increasing of the literature on this argument has been seen in the recent years. Several experimental methods, such as, for instance, thermogravitational columns,^{18–20} diffusion cells,²¹ thermal field flow fractionation,⁵ and, most recently, thermal diffusion forced Rayleigh scattering (see, for instance, Refs. 22 and 23) have been used to measure the Soret coefficient. Nevertheless, measuring S_T remains a difficult task. This is mainly due to the fact that thermally driven flows are minor effects, several orders of magnitude smaller than concentration driven flows and convective motions.²⁴ The problems due to convective motions can be reduced in microgravity experiments.^{25,26} For these reasons very sensitive methods are necessary to obtain reliable measures for the Soret coefficient. In general, the Soret coefficient is small ($<10^{-2}$ K⁻¹) for gas or liquid mixtures of molecular species, while for disperse systems (colloid, polymer, surfactant dispersions) it is often much larger.

From the theoretical point of view one also has to face many difficulties and ambiguous situations have been found. If the interaction between particles is vanishing, one has that $S_T=1/T$ (see, for instance, Ref. 10 for the derivation) but this

^{a)}Dedicated to Andrea.

^{b)}Author to whom correspondence to be addressed. Electronic mail: ermy@crs4.it.

result is seldom correct for actual systems. For dilute gases, thermal diffusion is described using the Chapman–Enskog solution²⁷ of the Boltzmann equation and the behavior of some mixtures can be predicted. In such a situation, if the species have roughly equal masses, the heavier molecules diffuse toward the colder region and then the larger molecules diffuse into the colder region. For very large mass ratios, thermal diffusion may increase by several orders of magnitude increasing the light component mole fraction and experimental values for S_T in general agree with these rules.²⁷ Expressions for the thermal diffusion factor ($\alpha_T = TS_T$) in molecular gasses (see Ref. 28, and references therein) have been obtained. In dense gases and liquid mixtures the situation is less favorable. Lopez de Haro, Cohen, and Kincaid^{29–32} have derived and discussed expressions for the transport coefficient in dense liquid mixtures based on a consistent generalization of the Enskog theory to multicomponent hard-sphere mixtures called the revised Enskog theory (RET), which should help in understanding cross-transport phenomena although they insist on the sensitivity of S_T to the interaction potential and consider that the RET results must not be seen as a quantitative tool.³² More recently, other approaches have been proposed, based on elementary hydrodynamic and Brownian motion model.^{33,34} The complete description of the studies concerning thermal diffusion is out of the scope of this paper and for a recent review the reader is referred to Ref. 4.

During the 1980s, many approaches based on irreversible thermodynamics and nonequilibrium statistical mechanics have been developed to compute the Soret coefficient in binary mixtures using molecular dynamics (MD) methods (for a short summary, see Ref. 35, and references therein). The applications of MD simulations to the study of thermal diffusion have been devoted to the development of methodologies^{36–39} and to the study of the Lennard-Jones (LJ) mixtures.^{3,24} There have been also attempts to compute the Soret coefficient in molecular liquids.^{35,40–44} An important contribution to the study of thermal diffusion in high density liquids has been presented by Müller-Plathe.^{24,39} In particular he has proposed a nonequilibrium molecular dynamics method for generating temperature gradients, by imposing a heat flux, initially indicated with “reverse- nonequilibrium molecular dynamics (NEMD)” (RNEMD) and then with “boundary-driven-NEMD” (boundary-NEMD). For the sake of conciseness we shall use in the following the acronym RNEMD. In RNEMD, the simulation box is divided into N slabs perpendicular to the z direction. Slab 0 is defined as the “cold” slab and slab $N/2$ as the “hot” slab. Such a choice allows the periodic boundary conditions to be satisfied. The heat flux is generated by exchanging, for each species, the velocity vectors of the hottest particle in the cold slab with the coldest one in the hot slab. In the hypothesis that the coldest particles of the hot slab has less kinetic energy than the hottest one of the cold slab (normally satisfied, due to the broad form of the Maxwell-Boltzmann distribution), the exchange leads to an energy transfer from the cold slab to the hot one. The temperature therefore increases in the hot slab and decreases in the cold slab. The consequence is to establish a temperature difference between the two slabs

and a temperature gradient in the intermediate region. At the stationary state the (artificial) energy transfer is balanced by the heat flux from the hot slab to the cold one originated by the temperature gradient. The velocity exchange is done every N_{exch} simulation time steps, where N_{exch} is chosen (in a trial and error strategy) so that the temperature gradient is as small as possible with the constraint to show a clear (and numerically stable) concentration gradient. This exchange algorithm can present problems in case of dilute gaseous mixtures, due to the possibility that in one of the two exchanging slabs (cold and hot) a given component is absent. For such a situation, Nieto-Draghi and Avalos⁴⁵ have proposed a modification of the original algorithm in which the energy exchange is seen as an hypothetical elastic collision between two particles (the one with the largest kinetic energy in the cold slab and the one with the lowest kinetic energy in the hot slab) regardless of their nature. Given that the systems here considered are equimolar (*vide infra*) and in relatively dense state, the original implementation has been used.

It is now accepted that the thermodiffusion process has both kinetic contributions (due to selective collision interactions) and thermodynamic contributions (due to selective interactions between the species of the system): both contributions depend on the particle mass, on the nature and form of the interaction potential, and on the concentration of the components. The kinetic theory of dilute gasses^{27,32} has shown that S_T is more dependent on the characteristics of the interaction potential than the other transport properties. For this reason various authors have published studies concerning the dependence of S_T on the potential parameters. By using his algorithm, Müller-Plathe has studied both qualitative and quantitative aspects of thermal diffusion, investigating the influence of systematic variations of the physical parameters (mass, atomic diameter, interaction strength)^{24,46} with LJ potentials. Maghari and Yeganegi⁴⁷ have also considered the influence of LJ parameters on S_T in a system of particles of equal masses.

With the aim to contribute to the process toward a definition of a model of the thermodiffusion process, this paper concerns the study of the influence on S_T of both the temperature and the softness of the interaction potential.

In the present paper the Müller-Plathe algorithm³⁹ has been implemented into the commercial code M.DYNAMIX⁴⁸ and thermodiffusion has been studied considering a model system composed by two atomic species experiencing only repulsive potentials (both for the intra- and interatomic interaction). The potentials used in this study can be considered as derived from the LJ one, neglecting the attractive part and systematically changing the exponent n of the repulsive term. In particular, we have chosen a system resembling to an equimolar binary mixture of particles, with LJ parameters (mass, σ and ϵ) corresponding to those of argon and krypton. The aim of the present work is to look at the dependence of S_T on the interaction softness and not to reproduce experimental results on the argon and krypton liquid mixture, for which theoretical study have been published.^{37,42,49,50}

The rest of the paper is organized as follows: in Sec. II the computational details are described; in Sec. III general considerations regarding the extraction of S_T from the MD

simulation data are reported; in Sec. IV the effect of the variation of the exponent of the repulsive potential n and of the temperature on the value of the Soret coefficient S_T is studied; and finally in Sec. VI we shall summarize the relevant results here obtained.

II. COMPUTATIONAL DETAILS

A system composed of 750 argonlike atoms and 750 kryptonlike atoms, in an orthorhombic periodic cell of size $90 \times 30 \times 30 \text{ \AA}^3$ is considered in the present study. The interaction between the atoms is supposed to be purely repulsive and, in practice, it can be seen as obtained from the LJ potential by neglecting the attractive part and varying the exponent n (equal to 12 in the LJ potential), as shown in Eq. (1),

$$U_{ij}^n(r_{ij}) = 4\epsilon_{ij} \left(\frac{\sigma_{ij}}{r_{ij}} \right)^n; \quad n = 1, 3, 6, 9, 12. \quad (1)$$

In this equation $U_{ij}^n(r_{ij})$ is the interaction potential of two atoms i and j , r_{ij} their distance, ϵ_{ij} and σ_{ij} two parameters related, in the LJ potentials, to the depth of the potential well and to the distance of the potential minimum, respectively. For the argon-argon interaction the LJ parameters are $\epsilon_{\text{ArAr}} = 1.00 \text{ kJ/mol}$ and $\sigma_{\text{ArAr}} = 3.405 \text{ \AA}$, while for krypton-krypton they are $\epsilon_{\text{KrKr}} = 1.39 \text{ kJ/mol}$ and $\sigma_{\text{KrKr}} = 3.633 \text{ \AA}$.²⁴ In the case $i \neq j$, ϵ_{ij} and σ_{ij} follow the Lorentz–Berthelot rule, so that

$$\epsilon_{ij} = \sqrt{\epsilon_{ii}\epsilon_{jj}}, \quad (2)$$

$$\sigma_{ij} = \frac{\sigma_{ii} + \sigma_{jj}}{2}. \quad (3)$$

In the following, n ranges from 1 to 12, assuming the values 1, 3, 6, 9, and 12. With $n=1$ the interaction has the form of a “pseudocoulombian potential” (note that in the systems there are not actual charges), while for $n=12$ the interaction can be considered an “almost-hard-sphere” potential. These kind of potentials are also called soft-sphere potential. The fluids composed of such particles have been the subject of a number of studies and in particular they have been used in a molecular dynamic study of the n dependence of the self-diffusion coefficient, shear viscosity, bulk viscosity, and thermal conductivity (see Ref. 51, and references therein). A comparison between the LJ potentials and those here used for $n=1$ and $n=12$ is shown in Fig. 1 for the interaction Ar–Kr.

In the MD simulations (both equilibrium and nonequilibrium MD), the time step Δt is 1 fs. For the potentials with $n \neq 1$, the chosen cutoff distance, r_c , corresponds to an energy truncation, E_c , of the order of 10^{-4} kJ/mol , except for the case with $n=3$ where the energy truncation is of order 10^{-2} kJ/mol . In this case r_c corresponds to half of the shorter box length, a limit imposed by the periodic boundary conditions. A better cutoff should need larger box size and, therefore, larger number of particles, with too expensive computational efforts. The values of r_c for the potential with $n \neq 1$ are reported in Table I.

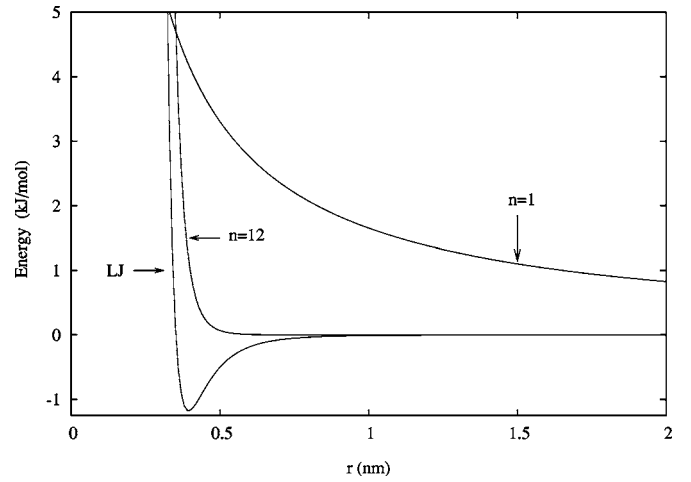


FIG. 1. Comparison between the Lennard-Jones potential and the repulsive potentials with $n=12$ and $n=1$ for the cross interaction Ar–Kr.

The repulsive potential with $n=1$ has been treated as an electrostatic interaction between particles with zero charge, with the long-range interaction calculated using the Ewald sum. In the Ewald method, the intermolecular coulomb forces are divided into long range and short range components. The long range part is calculated in the reciprocal space, while the short range part is treated alongside with LJ forces. The convergence of both parts is controlled by three parameters: the two cutoff radii in the real and reciprocal spaces and the convergence parameter (denoted as α) regulating the convergence of both the real and reciprocal parts of the Ewald sum. In the M.DYNAMIX program, these parameters are set in the following way: first, the cutoff radius in real space, R_{cut} , has to be specified explicitly, then, the convergence parameter α is specified as the product αR_{cut} . This product entirely determines the precision of the real-space part, $\text{erfc}(\alpha R_{\text{cut}})$, which must be small enough, and in our case is 2.2×10^{-5} ($R_{\text{cut}} = 8.7 \text{ \AA}$, $\alpha R_{\text{cut}} = 3.0$). The third parameter, $\text{FEXP} = (k_{\text{max}} \pi / \alpha L_{\text{box}})^2$, determines the value of the cutoff in the reciprocal space, k_{max} , and thereby the precision of the reciprocal part of the Ewald sum, which is equal to $\exp[-\text{FEXP}]$, in our case 1.2×10^{-4} . Fictitious charges have been assigned to the two particles species, satisfying the condition

$$4\epsilon_{ij}\sigma_{ij} = q_i q_j. \quad (4)$$

Let us note that in such a way the charge assigned to an atom depends on the nature of the atom it is interacting with.

Moreover, for the case with $n=1$, smaller box size and number of particles have been considered to have a reasonable computational time. In particular, the total number of particles is 300 (150 argon atoms and 150 krypton atoms) and the box size is $52.6 \times 17.6 \times 17.6 \text{ \AA}^3$.

TABLE I. Cutoff distance at various potentials.

n	3	6	9	12
$r_c(\text{\AA})$	14.9	14.9	9.211	7.242

The RNEMD simulation, on which statistic information are collected, is always performed after two runs. The first one is an equilibrium MD simulation 2×10^6 time steps long and the second one is a RNEMD simulation, other 2×10^6 time steps long. In this way we are sure that the system in the final RNEMD simulation is at the steady state. This assumption has been verified by analyzing the behavior of various quantities (the total energy, the concentration profile, the temperature profile, the energy flux), which are expected to be constant during the final RNEMD simulation. In the final RNEMD calculation, data are collected over a simulation 10^7 time steps long.

A particular role is played by the temperature used in the equilibrium MD simulation because it represents the temperature around which the temperature gradient develops, that is a sort of average temperature in the RNEMD steps. It is indicated in the following with T_{eq} . The equilibrium MD simulations have been performed for each repulsive potential at the following values of T_{eq} : 120, 250, 400, 600, and 800 K. The aim is to cover a wide range of temperatures and to have the thermodiffusion coefficient as a function of both the potential and the temperature.

In RNEMD the simulation box has been divided into $N_s=12$ slabs of equal thickness, perpendicular to the z direction. Slab 0 is defined as the cold slab and slab 6 as the hot slab. The values for N_s have been chosen so that reasonable statistics can be expected inside the slabs: on average there are 125 particles in each slab, except for the cases with $n=1$, where the average number of particles is 25. No appreciable variations have been observed in the RNEMD simulations for (relatively small) variation of the box size for $n=1$. The dependence of the box size on the results has been evaluated only for the case with $T_{\text{eq}}=120$ K, at the price of a very high computational effort. The small differences found have motivated the choice of a smaller box size.

The value of N_{exch} , the number of simulation steps between two successive velocity exchanges, is calibrated in order to produce similar temperature gradients in all simulations. Therefore, for $n \leq 9$ $N_{\text{exch}}=250$, otherwise it is 350.

Because of the symmetry of the simulation box, average values of temperature and composition are calculated between slab $N_s/2-i$ and $N_s/2+i$, with $i=1,5$, having excluded the first and central slabs because of the unphysical effects due to the particle exchange procedure. Hereafter species 1 refers to kryptonlike atoms.

III. CALCULATION OF THE SORET COEFFICIENT FROM THE CONCENTRATION AND TEMPERATURE PROFILES

Following the paper of Reith and Müller-Plathe,²⁴ the thermal diffusion is phenomenologically expressed as

$$J_1 = -D_{12}\rho \left[\left(\frac{\partial w_1}{\partial z} \right) + S_T w_1 (1 - w_1) \left(\frac{\partial T}{\partial z} \right) \right], \quad (5)$$

where D_{12} is the Fickian diffusion coefficient, the temperature gradient and the flux J of all species are assumed in the z direction, ρ is the average mass density, and $w_1 = x_1 m_1 / (x_1 m_1 + x_2 m_2)$ is the weight fraction of species 1 (x_k

denoting the mole fraction of species k). Equation (5) is valid in the frame of the linear nonequilibrium thermodynamics, where it is postulated that the fluxes depend linearly on the generalized forces.⁵² Under the effect of a constant temperature gradient, the system reaches a nonequilibrium steady state ($J_1=0$) and a stable concentration profile is therefore established so that Eq. (5) reduces to

$$\left(\frac{\partial w_1}{\partial z} \right) + S_T w_1 (1 - w_1) \left(\frac{\partial T}{\partial z} \right) = 0. \quad (6)$$

Taking account of the relationship between the weight fractions and the molar fractions (a quantity experimentally more accessible), the Soret coefficient can be expressed as

$$S_T = - \frac{1}{x_1(1-x_1)} \left(\frac{\partial x_1}{\partial z} \right) \left(\frac{\partial T}{\partial z} \right)^{-1}, \quad (7)$$

with positive values of S_T indicating that species 1 tends to accumulate in the cold regions of the simulation box. It is common practice to choose as species 1 the heavier species. With this notation, in many cases S_T has a positive value in accordance with the dilute gases result.²⁷ For instance, polymers in solution conform to this rule, with relatively few known exceptions. However, various situations have been described where S_T is negative and in some case one can even observe a sign change of S_T by small modifications of the mixture composition and of the temperature (see Sec. V). This behavior is observed also in the present paper and fully described in Sec. IV B.

Let us first comment on the integration of Eq. (6) and which form one can expect for the composition profile at the steady state. This is relevant in order to correctly analyze the results of RNEMD. With the hypothesis that S_T depends only on T , Eq. (6) (written with x_1 as the unknown function) can be integrated obtaining

$$x_1(T) = \frac{1}{1 + A e^{\int S_T dT}}, \quad (8)$$

from which $x_1(z)$ is easily found if $T(z)$ is known. The parameter A is defined by a boundary condition (for instance the value of the integral of x_1 over the full interval of z or the value of x_1 at a given z). In the case of a dependence of S_T on x_1 the problem is more complicated. However, in the present study (see Sec. IV) we have found that S_T depends only on T (at least in the range of x_1 explored by our simulations) and Eq. (8) gives the correct profile of x_1 .

In both experimental and theoretical studies one normally observes linear temperature profiles. This is essentially due to the fact that the Dufour effect is very small and that the thermal conductivity is almost constant in the range of temperature and composition found in the system. In the following we therefore assume for the temperature the form $T = a + bz$. A second hypothesis is normally assumed in literature: S_T does not depend on T in the range of temperatures spanned in the system. While this assumption seems reasonable in the experimental works, where small variations of T are normally generated, it can be questionable in RNEMD simulations where ΔT is of the order of $10^1 - 10^2$ K. However, assuming these hypothesis for T and S_T , $x_1(z)$ is

TABLE II. Temperatures corresponding to the hot and cold slabs (T_{\max} and T_{\min} , in K) and corresponding compositions, for the various repulsive potentials and with different T_{eq} computed in the RNEMD simulations.

T_{eq}		$n=1$		$n=3$		$n=6$		$n=9$		$n=12$	
		Hot	Cold								
120	T	177	58	171	69	156	83	153	87	146	94
	x_{Kr}	0.4857	0.5274	0.411	0.6137	0.4033	0.6104	0.4123	0.5994	0.4275	0.5797
200	T	286	103								
	x_{Kr}	0.5077	0.4961								
250	T			362	138	332	170	319	182	301	200
	x_{Kr}			0.4435	0.5710	0.4283	0.5822	0.4178	0.5846	0.4356	0.5720
300	T	411	178								
	x_{Kr}	0.5138	0.4867								
400	T	550	235	575	223	536	269	511	291	480	321
	x_{Kr}	0.5237	0.4797	0.4728	0.5406	0.4322	0.5813	0.4237	0.5853	0.4466	0.5646
600	T	790	400	848	348	807	403	770	438	719	484
	x_{Kr}	0.5193	0.4808	0.4824	0.5217	0.4485	0.5574	0.4350	0.5703	0.4449	0.5567
800	T	1000	578	1113	484	1074	540	1026	585	956	650
	x_{Kr}	0.5118	0.4908	0.4973	0.5057	0.4518	0.5540	0.4368	0.5636	0.4531	0.5488

$$x_1(z) = \frac{1}{1 + A' e^{S_T b z}}, \quad (9)$$

where $A' = A e^{S_T a}$. One notes that $x_1(z)$ is not a linear function of z , even with a linear temperature profile and with a constant value of S_T . The product $S_T b z$ is, however, in general small (S_T is often of the order of 10^{-3} K^{-1} and the temperature variation, bz , does not exceed $1-2 \times 10^2 \text{ K}$) and one can use a Taylor expansion of $x_1(z)$. To the first order in the product $S_T b z$, Eq. (9) becomes

$$x_1(z) \approx \frac{1}{1 + A'} - \frac{A'}{(1 + A')^2} S_T b z \quad (10)$$

and x_1 is, at this point, linear in z .

Summarizing, the request for x_1 to be linear is based on the hypothesis:

- S_T is constant with respect to T and x_1 and
- the product $S_T b z$ is small.

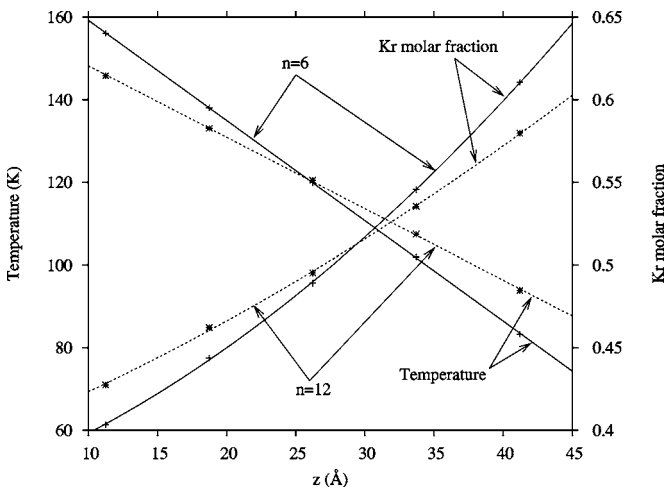


FIG. 2. Temperature and composition gradients corresponding to $T_{\text{eq}} = 120 \text{ K}$ for the cases with $n=6$ and $n=12$.

On the basis of the earlier considerations, let us now consider how S_T can be extracted from the RNEMD calculations. In RNEMD the temperature and the composition profiles are known for a set of z values corresponding to the center of each slab of the simulation box and they normally are fitted by straight lines [say $T(z) = a + bz$, $x_1(z) = c + dz$, see, for instance, Refs. 24, 35, and 66], therefore obtaining

$$\left(\frac{\partial x_1}{\partial z} \right) \left(\frac{\partial T}{\partial z} \right)^{-1} \approx \frac{d}{b}. \quad (11)$$

Another approximation is normally adopted concerning x_1 (which is a function of z) in the fraction $[x_1(1-x_1)]^{-1}$: it is substituted by its mean value (\bar{x}_1) (see, for instance, Refs. 24 and 45), thus reducing Eq. (7) to

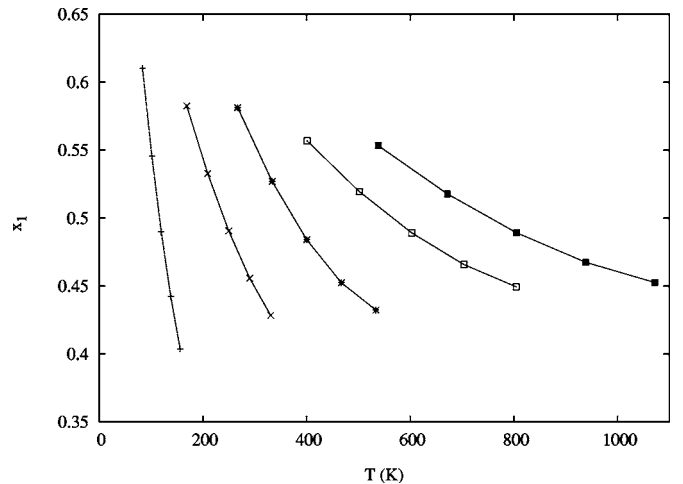


FIG. 3. Composition (x_1) vs temperature in the simulations with $T_{\text{eq}} = 120$ (+), 250 (x), 400 (*), 600 (□), and 800 K (■) for the potential with $n=6$. The points correspond to the fitted values at the center of the five slabs used for the fitting procedure.

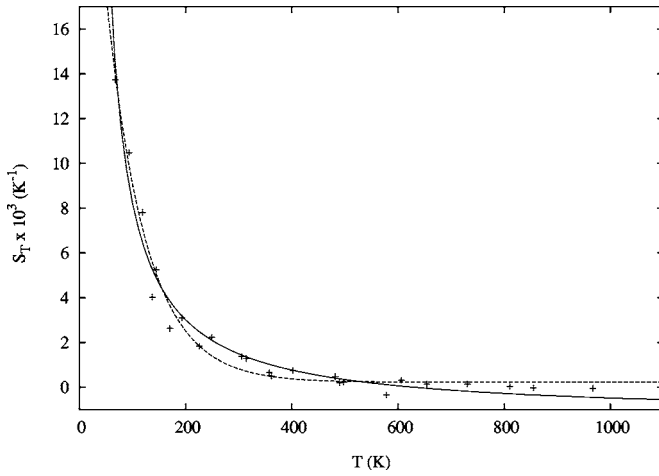


FIG. 4. Soret coefficient as a function of the temperature for $n=3$: computed points (at the center of the slab, for each T_{eq} , indicated with +) and fitting functions [$S_T = a + b/(T - c)$, full line; $S_T = a + e^{-(T-c)/b}$, dashed line].

$$S_T \approx -\frac{1}{\bar{x}_1(1-\bar{x}_1)} \frac{d}{b}. \quad (12)$$

Let us note that this last approximation can have sizable effects: considering for instance a case where $\bar{x}_1 = 0.25$ and x_1 assumes values in the interval $0.20-0.30$, then $[x_1(1-x_1)]^{-1}$ assumes values in the range $4.76-6.25$ while with \bar{x}_1 one gets 5.33 . On the other hand, using for instance, Eq. (12) with x_1 depending on z , gives variable values for S_T even in a linear regime (x_1 and T linear in z).

One may wonder whether all these approximations and assumptions are necessary and in particular if it is strictly mandatory to look for linear composition profiles in RNEMD. In particular cases, for instance, this request is almost impossible to satisfy: in Sec. IV B the case of a sign change of S_T in the temperature range found in the system, leads to nonlinear x_1 profiles. Obviously, one can perform the simulation at a different T_{eq} , but this is an annoying constraint.

Actually Eq. (7) allows the definition of S_T once $T(z)$ and $x_1(z)$ are defined. As already said, in RNEMD simulations temperature and composition are known as single value for each slab and assigned to z_i (the center of slab i). They can be analytically fitted as a function of z (using straight line or other functions), then Eq. (7) allows the definition of S_T for each value of z_i through the analytical derivatives of T and x_1 in z_i and using the value $x_1(z_i)$. One can thus obtain S_T for each value of $T(z_i)$ in the range $T_{\text{max}} - T_{\text{min}}$ (that is in the range $x_1^{\text{max}} - x_1^{\text{min}}$), where T_{max} and T_{min} (x_1^{max} and x_1^{min}) are the maximum and minimum temperature (molar fraction) found in the various slabs.

In the present work such a strategy has been adopted: in order to carefully fit the concentration profiles, without assuming a linear behavior, very stable values of x_1 for each slab are necessary. For this reason less slabs and more particles (both choices increasing the number of particles for each slab) than recommended have been considered. Within this strategy one can explore the possibility to have nonlinear concentration profiles.

The linear response regime to the energy flux crossing

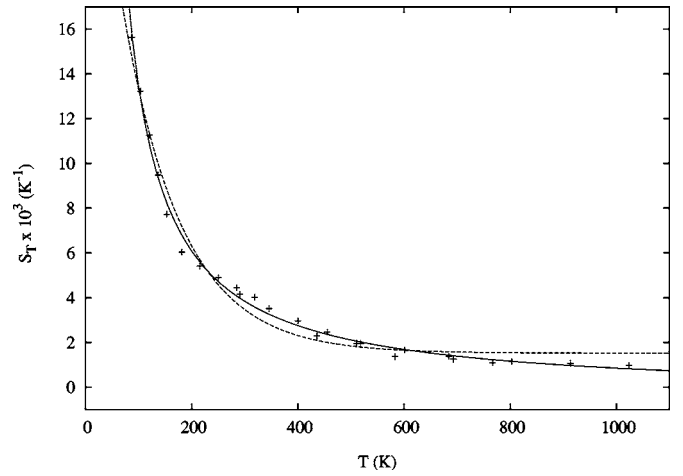


FIG. 5. Soret coefficient as a function of the temperature for $n=9$: computed points (at the center of the slab, for each T_{eq} , indicated with +) and fitting functions [$S_T = a + b/(T - c)$, full line; $S_T = a + e^{-(T-c)/b}$, dashed line].

the system is guaranteed by the linearity of the temperature profile, while for the concentration one can expect more complicate shapes (even in the frame of linear nonequilibrium thermodynamics), following the dependence of S_T on T and x_1 . In particular, a marked nonlinearity in the concentration profile indicates that S_T shows significant changes in the range of temperature and/or concentration found in the system and in a single simulation one can expect to have more information on the dependence of S_T on T and x_1 . To this end, strong temperature gradients are generated in our simulations, always taking care, however, to have a linear response of the system to the perturbation (linear temperature profiles).

IV. DEPENDENCE OF S_T ON THE EXPONENT OF THE REPULSIVE POTENTIAL n AND THE TEMPERATURE

The maximum and minimum value of the temperature gradients, together with the corresponding mixture compositions, are indicated in Table II for each value of n and T_{eq} .

In order to be sure that the development of the concentration gradients are originated by the thermodiffusion process and that they are not due to changes of phase, for each repulsive potential and T_{eq} , equilibrium MD simulations have been performed at T_{max} and T_{min} and at the corresponding composition. The results of such simulations confirm that no change of state occurs and that the formation of the concentration gradient is actually due to thermodiffusion. From the analysis of the results of the simulations at various n and T_{eq} , we have found that temperature gradients have always a linear behavior, thus confirming that the response of the system to the unphysical velocity exchange is linear. Moreover, such simulations confirm that the assumption of local thermal equilibrium is satisfied.

In the next two subsections the case of the potentials with $n \geq 3$ and the one with $n=1$ are considered separately.

TABLE III. Dependence of the Soret coefficient of the temperature for the potential with $n \geq 3$: parameters of the analytical interpolation. rms=root-mean-square of residuals.

n	a	b	c	rms
		$S_T(T) = a + b/(T - c)$		
3	$-1.279 \times 10^{-3} \pm 0.275 \times 10^{-3}$	0.783 ± 0.093	17.55 ± 6.28	0.651×10^{-3}
6	$-1.091 \times 10^{-3} \pm 0.252 \times 10^{-3}$	1.214 ± 0.105	14.69 ± 6.17	0.501×10^{-3}
9	$-0.377 \times 10^{-3} \pm 0.158 \times 10^{-3}$	1.213 ± 0.070	12.29 ± 4.43	0.297×10^{-3}
12	$-1.000 \times 10^{-3} \pm 0.247 \times 10^{-3}$	1.713 ± 0.140	16.18 ± 8.67	0.354×10^{-3}
		$S_T(T) = a + e^{-(T-c)/b}$		
3	$0.222 \times 10^{-3} \pm 0.150 \times 10^{-3}$	74.05 ± 4.88	-250.1 ± 22.3	0.555×10^{-3}
6	$0.968 \times 10^{-3} \pm 0.157 \times 10^{-3}$	96.86 ± 5.62	-324.7 ± 24.9	0.519×10^{-3}
9	$1.519 \times 10^{-3} \pm 0.190 \times 10^{-3}$	111.0 ± 8.11	-392.9 ± 36.4	0.589×10^{-3}
12	$1.296 \times 10^{-3} \pm 0.129 \times 10^{-3}$	142.1 ± 6.32	-527.4 ± 28.2	0.343×10^{-3}

A. The potentials with $n \geq 3$

For the repulsive potentials with $n \geq 3$, concentration gradients are normally better described with a quadratic shape, as shown, for example, in Fig. 2, for the RNEMD simulations with $n=6$ and $n=12$ at $T_{\text{eq}}=120$ K.

For a given n , each simulation (characterized by the value of T_{eq}) describes a line in the plane x_1 versus T . An example is reported in Fig. 3 for the case $n=6$.

The calculation of the Soret coefficient is performed at the z values corresponding to the center of the five physically relevant slabs, thus obtaining a set of points in the space $x_1, T, S_T(x_1, T)$. The advantage of the approach here presented, and adopted for the extraction of S_T from the NEMD data, is evident by considering an example. For instance with $T_{\text{eq}}=120$ K and $n=6$, the direct use of Eq. (7) with the derivatives computed from the interpolated x_1 and T functions gives: $S_T(0.610, 83.5) = 15.91 \times 10^{-3} \text{ K}^{-1}$, $S_T(0.546, 101.7) = 13.36 \times 10^{-3} \text{ K}^{-1}$, $S_T(0.490, 119.9) = 11.36 \times 10^{-3} \text{ K}^{-1}$, $S_T(0.443, 138.0) = 9.60 \times 10^{-3} \text{ K}^{-1}$, and $S_T(0.404, 156.2) = 7.87 \times 10^{-3} \text{ K}^{-1}$. From the same set of data, the use of Eq. (12) (as normally done in all NEMD simulation) gives a unique value for the Soret coefficient, that is $S_T(0.5, 120) = 11.36 \times 10^{-3} \text{ K}^{-1}$, which closely corresponds to the result obtained earlier for the values of $x_1=0.490$ and $T=119.9$ K.

The 25 values of S_T have been fitted as function of both x_1 and T , with various trial functions. For each value of the potential exponent n we have found that S_T shows a negligible dependence on x_1 , at least in the interval of composition explored by our simulations. Thus, S_T has been fitted as a function of only T using the following two trial functions:

$$S_T = a + \frac{b}{T - c} \quad (13)$$

and

$$S_T = a + e^{-(T-c)/b}. \quad (14)$$

Iacopini *et al.*⁵³ have used a function similar to Eq. (14) to fit S_T . Both functions give satisfactory results, with the exponential one having a slightly worse behavior: two examples, for the case $n=3$ and $n=9$, are reported in Figs. 4 and 5, respectively.

The best parameters of both fitting functions are reported for all $n \geq 3$ in Table III.

A global overview of the variation of S_T with respect to T for all n is reported in Figs. 6 and 7, with S_T expressed using Eqs. (13) and (14), respectively.

For all n the Soret coefficient is positive and large at low temperature, it decreases rapidly with increasing T , reaching low values ($< 2 \times 10^{-3} \text{ K}^{-1}$) for T greater than 500–600 K. The negative values found for large T with $n=3$ and Eq. (13) are an artifact of the fitting procedure, as can be seen in Fig. 4. Increasing n leads to an overall (moderate) increase of S_T . The values of S_T for an ideal gas mixture ($1/T$) is also reported in Fig. 6 for comparison. It is apparent that this function closely resembles the profiles of the computed S_T for all n , the case $n=3$ being the farthest.

Let us note that using $S_T=1/T$, Eq. (8) becomes

$$x_1(T) = \frac{1}{1 + AT} \quad (15)$$

and if $T=a+bz$ one has

$$x_1(z) = \frac{1}{1 + A(a + bz)}. \quad (16)$$

As a conclusion, we have found in this section that our model system with $n \geq 3$ behaves, with relatively small de-

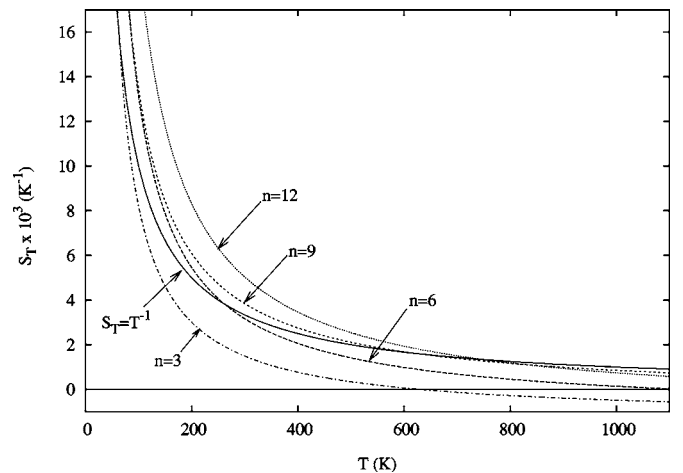


FIG. 6. Soret coefficient as a function of the temperature: fitting functions for all $n > 3$. The fitting functions have the form $S_T = a + b/(T - c)$. In full line the zero line and the function $S_T = 1/T$ of an ideal gas mixture have been added for comparison.

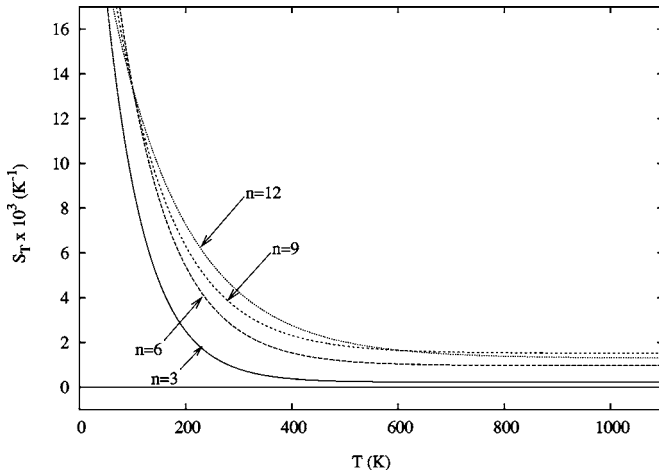


FIG. 7. Soret coefficient as a function of the temperature; fitting functions for all $n > 3$. The fitting functions have the form $S_T = a + e^{-(T-c)/b}$. In full line the zero line has been added for comparison.

viations depending on n , as an ideal gas mixture.

B. The potentials with $n=1$

The RNEMD simulations with the pseudocoulombian interaction potential have shown peculiar results. A first difference with the other potentials has been found at high T ($T_{\text{eq}} \geq 300$ K), where (small) negative S_T have been computed. As in the previous simulations, the temperature values show a linear behavior and the x_1 profile is well fitted by a parabolic function, but species 1 accumulate in the hot region.

At low temperature ($T_{\text{eq}} = 120$ and 200 K), while T remains linear, x_1 shows surprising shapes. Figure 8 reports, for instance, the case $T_{\text{eq}} = 200$ K. The temperature profile is linear, as previously found, but one promptly notes that while for the first four points x_1 decreases increasing z , for the last point the opposite occurs. This is an indication of a sign change of the Soret coefficient at a temperature close to 150 K. In this case the use of a parabolic function for x_1 in the fitting procedure gives poor results: as said in Sec. IV we

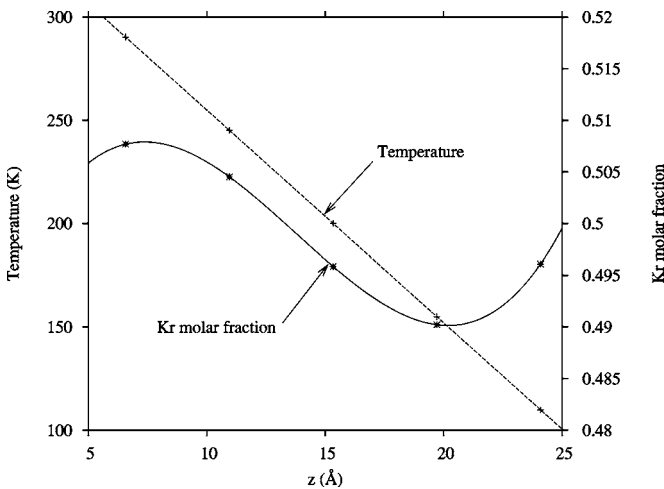


FIG. 8. Temperature and composition gradients corresponding to $T_{\text{eq}} = 200$ K for the cases with $n=1$.

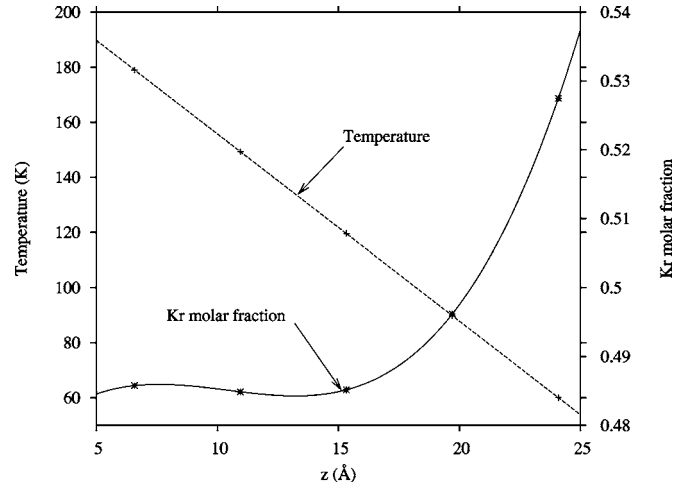


FIG. 9. Temperature and composition gradients corresponding to $T_{\text{eq}} = 120$ K for the cases with $n=1$.

adopt the strategy to perform a close fitting of both x_1 and T , so a cubic function has been considered and reported in Fig. 8.

Analogously, at $T_{\text{eq}} = 120$ K one notes an unusual composition shape, as it is apparent in Fig. 9. In this case the first three points show an almost constant composition, while for the last two points x_1 increases rapidly. Again this is consistent with a sign change of S_T at $T \approx 120$ – 150 K, with S_T being strongly positive for lower T .

The interpolated x_1 functions (cubic for $T_{\text{eq}} = 120$ and 200 K, parabolic in the other cases) have been used to obtain S_T at the center of the five relevant slabs. As found for $n \geq 3$, the S_T values show a negligible dependence on the composition, while the dependence on the temperature is marked. The S_T values have been fitted, as function of T , with various trial expression: the best results have been obtained with a Morse and a LJ profile

$$S_T = \gamma \{ [1 - e^{-\alpha(T-\beta)}]^2 - 1 \}, \quad (17)$$

$$S_T = \gamma \left[\left(\frac{\alpha}{T-\beta} \right)^{12} - \left(\frac{\alpha}{T-\beta} \right)^6 \right]. \quad (18)$$

The S_T values computed for the five T_{eq} and the two fitting functions are reported in Fig. 10. The fitting parameters are $\gamma = 0.757 \times 10^{-3}$, $\alpha = 0.751 \times 10^{-2}$, and $\beta = 242.4$ for the Morse function and $\gamma = 2.864 \times 10^{-3}$, $\alpha = 813.0$, and $\beta = -663.3$ for the LJ function.

From Fig. 10 one notes that some points remain quite far from the interpolated curve: in particular two points are slightly above the zero line in an interval of T where all the other points are negative. These two values are computed in the first slab for the simulation with $T_{\text{eq}} = 120$ and 200 K, that is, the points with $z = 6.57$ in Figs. 8 and 9. Such values for S_T are clearly influenced by the derivative of the fitting function chosen for x_1 and by its incorrect behavior at low z , leading an artificial sign change. The exclusion of these two points from the fitting procedure leads to a negligible modification of the fitting functions and therefore they have been kept.

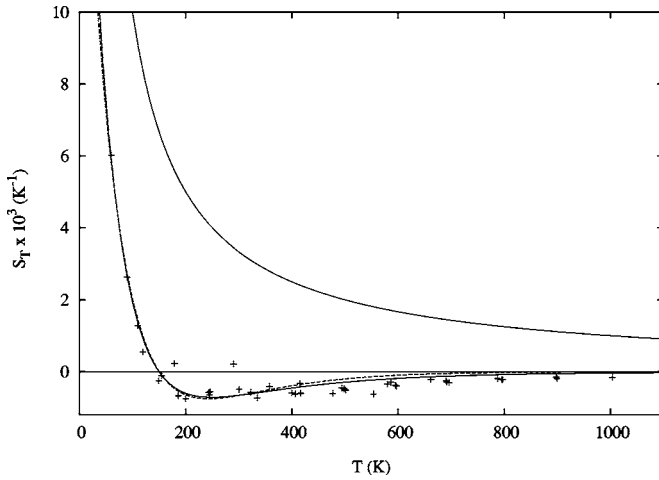


FIG. 10. Soret coefficient as a function of the temperature: computed points (at the center of the slab, for each T_{eq} , indicated with +) and fitting functions (Lennard-Jones, full line; Morse, dashed line). In full line the zero line and the function $S_T=1/T$ of a ideal gas mixture have been added for comparison.

Both fitting functions give a consistent description of the dependence of S_T on T : it is positive and large for low T and it rapidly decreases increasing T . For a temperature of 150.1 K (Morse) or 149.7 K (LJ) there is a sign change and S_T becomes negative. Close to 250 K S_T reaches a minimum and for larger T it slowly goes to zero. Actually the computed points indicate that S_T remains almost constant in the range of temperatures between 250–500 K, but the fitting functions do not describe this behavior. A similar dependence on T of S_T has been observed also in the study of polymer solution with a two-chamber lattice model (see Fig. 3 of Ref. 54) where both situations here described (positive and monotonically decreasing with $n \geq 3$ and change of sign with $n = 1$) has been found by changing the parameters of the model.

In order to verify the correctness of the analytical expression of $S_T(T)$, one can use the fitting functions [Eqs. (17) and (18)] in Eq. (8), obtaining

$$x_1(z) = \frac{1}{1 + A e^{\gamma/\alpha [2e^{-\alpha(T(z)-\beta)} - (1/2)e^{-2\alpha(T(z)-\beta)}]}} \quad (19)$$

for the Morse case and

$$x_1(z) = \frac{1}{1 + A e^{\gamma[-\alpha/11(\alpha(T(z)-\beta))^{11} + \alpha/5(\alpha(T(z)-\beta))^5]}} \quad (20)$$

for the LJ one. These two expressions are plotted for the case $T_{\text{eq}}=120$ K in Fig. 11 together with the values of x_1 obtained from the RNEMD simulation. The parameter A is obtained imposing that x_1 in Eqs. (19) and (20) is equal to the RNEMD value of the first slab. Similarly, Fig. 12 reports the results at $T_{\text{eq}}=200$ K: in this case the second RNEMD point has been chosen for the determination of A .

The agreement of the x_1 profile described by Eqs. (19) and (20) and the RNEMD values is very good: in both cases the clear nonlinear behavior of the RNEMD x_1 values is well reproduced. Moreover, the difference between the RNEMD x_1 values and the analytical profiles is an estimation of the uncertainty of the simulation results.

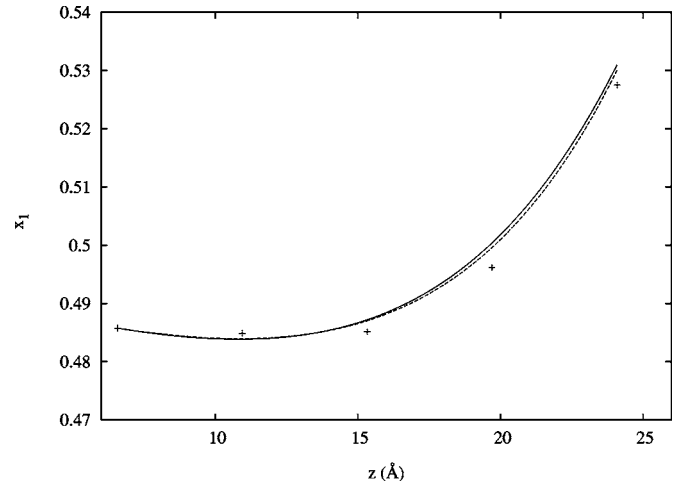


FIG. 11. Molar fraction of species 1 as a function of z for the case $T_{\text{eq}}=120$ K. The + points are computed from the RNEMD simulation. Full line: obtained from Eq. (19) (S_T described by a Morse function). Dashed line: obtained from Eq. (20) (S_T described by a Lennard-Jones function).

To the aim of further verifying the interpretative scheme here presented, we have performed a RNEMD simulation with $T_{\text{eq}}=150$ K, the temperature at which S_T change its sign. The calculated composition values and the profile obtained from Eqs. (19) and (20) are reported in Fig. 13 (A computed from the first simulated point).

The agreement is, in this case, slightly less satisfactory than with $T_{\text{eq}}=120$ and 200 K, but the variation of the computed x_1 values is qualitatively reproduced, thus confirming that the expressions found for S_T are correct.

Summarizing, we have obtained that, in case of repulsive pseudocoulombian interaction, the mixture here considered shows a thermodiffusion behavior with a strong qualitative difference with respect to the cases with $n \geq 3$. The Soret coefficient changes sign by modifying the temperature. To our best knowledge, this is the first example of such a behavior obtained in MD simulation with purely repulsive potentials. In the next section we shortly report some of the

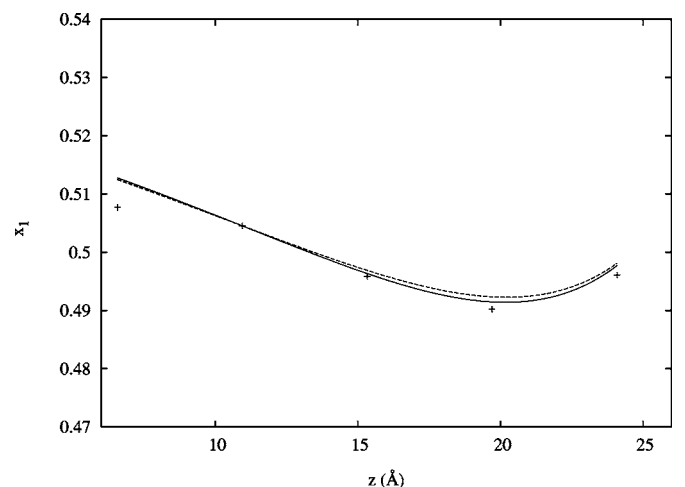


FIG. 12. Molar fraction of species 1 as a function of z for the case $T_{\text{eq}}=200$ K. The + points are computed from the RNEMD simulation. Full line: obtained from Eq. (19) (S_T described by a Morse function). Dashed line: obtained from Eq. (20) (S_T described by a Lennard-Jones function).

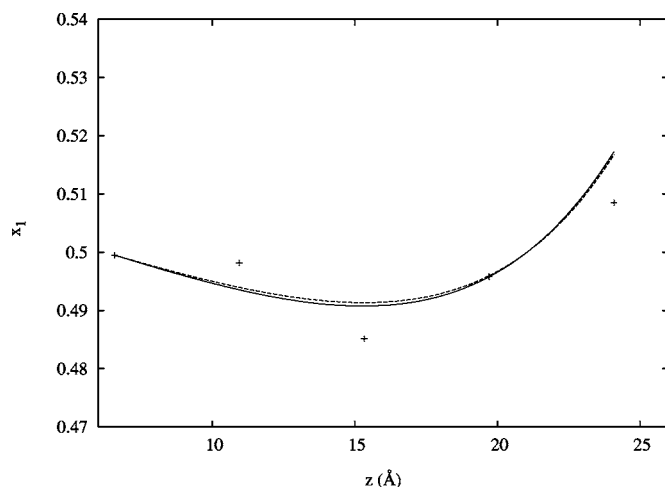


FIG. 13. Molar fraction of species 1 as a function of z for the case $T_{\text{eq}} = 150$ K. The + points are computed from the RNEMD simulation. Full line: obtained from Eq. (19) (S_T described by a Morse function). Dashed line: obtained from Eq. (20) (S_T described by a Lennard-Jones function).

published theoretical and experimental works where a sign change of S_T has been observed and we try to find analogies with the present results.

V. THE SIGN CHANGE OF S_T

Experimentally the sign change of S_T has been observed in two situations: when the composition of the mixture changes and when the temperature changes.

An example of the first situation is the ethanol/water mixture,⁵⁵ where a sign change of S_T is experimentally found by changing the mixture composition ($S_T=0$ for a mass fraction of water, w_{water} , equal to 0.71). Other alkanol water mixtures⁵⁶ and nonionic surfactants (hexaethylene glycol monododecyl ether) in water⁵⁷ also show this behavior.

In the case of polymers in solution, a negative S_T has been found for poly(vinyl alcohol) in water⁵⁸ and for poly(ethylene oxide) (PEO) in ethanol-rich ethanol/water mixtures.⁵⁹ In the last system, S_T has been found to show a sign change⁶⁰ by varying the solvent composition ($S_T=0$ for a weight fraction of water of 0.83). These results have also been qualitatively reproduced by a two chamber lattice model.⁵⁴ In theoretical simulation,³⁵ aqueous solutions of methanol, ethanol, acetone, and dimethyl-sulfoxide (DMSO) all show a sign change of S_T at a molar fraction $0.7 < x_{\text{water}} < 0.9$ passing from positive value for water-rich mixture to negative values for water-poor mixture. While in the case of the methanol/water and ethanol/water mixtures, such a behavior was experimentally known before the theoretical study,^{55,61} in the case of the acetone/water and DMSO/water mixtures the sign change has been theoretically predicted and further experimentally confirmed.²³ Another example is the benzene/cyclohexane mixture⁶² where S_T changes its sign at $x_{\text{benz}} \approx 0.7$. In this case the authors also observed that S_T splits into two additive contributions, one depending from the isotope composition and the other due to a “chemical” contribution. A sign change has also been observed in

charged colloid suspension.^{63–65} For other mixtures showing a change of sign modifying the composition, see Ref. 66, and references therein.

Iacopini *et al.*⁵³ have studied a set of dilute macromolecular and colloidal aqueous suspensions where a sign change is found by changing the temperature. They always found that below a given temperature S_T is negative and above it is positive. They call these systems “macromolecular tourist” given that they move toward the cold region when it is hotter than the “optimal” temperature and toward the hot region when it is colder. Given the evocative nature of such a terminology, we adopt it in the following, calling a system showing a sign change of S_T touristic if S_T has a positive slope with respect to T and nontourist if the slope is negative. In the same scheme we propose the name comfort temperature, T_{comf} , the temperature at which $S_T=0$. It is evident that in a binary mixture where there is a sign change of S_T as a function of T , always one of the two species acts as a tourist and the other as a nontourist. Let us remember, however, that S_T is usually computed with respect to the heavier species and with respect to this species the nomenclature of Iacopini *et al.*⁵³ is used in the following.

The suspension of octadecyl coated silica particles in toluene⁶⁷ show a change of sign as a function of both temperature and composition: with respect to temperature the colloidal particles show a touristic behavior with T_{comf} in the range 30–45 °C. It is worth noticing that for such a system the sign change is found for all investigated concentrations. A thermally induced sign change has been observed experimentally also in a semidilute solution of poly(*N*-isopropylacrylamide) in ethanol⁶⁸ with a nontourist behavior.

Another example of sign change is the dextran/water mixture:⁶⁹ Dextran behaves as a touristic macromolecule with $T_{\text{comf}}=45$ °C. Adding urea to the system leads to a decrease of T_{comf} which is 29.7 °C for a concentration of urea of 2 M and below the lowest measured temperature (≈ 15 °C) for a concentration of 5 M. This behavior is attributed to the breaking of the hydrogen network in pure water due to the urea molecules. Similar consideration on the origin of the sign change of S_T have been published for the water/ethanol mixture.⁵⁵ For such a system the authors have found that the hydrogen bond network of water is maintained up to $w_{\text{ethanol}}=0.18$: adding more ethanol results in a destruction of the network which is fully completed at $w_{\text{ethanol}}=0.6$. In the same paper the authors consider also the ternary system poly(ethylene oxide)/water/ethanol (a dilute solution of PEO in a mixed solvent water/ethanol). The S_T of PEO also shows a sign change with respect to the mass fraction of water in the solvent: S_T is vanishing for $w_{\text{water}}=0.83$, slightly larger than the case of the binary water/ethanol mixture. In the ternary system PEO/water/ethanol one also observes a sign change with respect to T for $w_{\text{water}}=0.80$, 0.82, and 0.85: in this case PEO behaves as a macromolecular tourist with T_{comf} decreasing if w_{water} increases.

The results reported in Sec. IV B indicate that the model system considered in the present work has a nontourist behavior with $T_{\text{comf}}=150$ K for purely repulsive interactions with $n=1$. On the contrary, for $n \geq 3$ (short range interac-

tions) the results agree with the general trend observed for hard sphere⁷⁰ and with the Chapman–Enskog theory,²⁷ that is the heavier component diffuses toward the colder region (positive Soret coefficient) and S_T has a $1/T$ dependence.

In Ref. 35 one can read that “in strongly nonideal or associating mixtures a change of sign of S_T with composition is almost invariably observed.” On the other hand, in general nonassociating fluids (for instance the n -pentane/ n -decane mixture⁴³) show a moderate variation of S_T with respect to composition. In the present study S_T does not show a relevant dependence on the composition (note, however, that the composition variations are small in our simulations) but we confirm that the presence of strong (long range) interactions strongly influences the Soret coefficient which shows, as a function of T , large deviation from the ideal gas case and a change of sign.

Finally, let us note that Nieto-Draghi *et al.*⁷¹ and Kita *et al.*⁵⁵ have found that the mixed interaction has to be stronger than the interactions between the pure components in order to describe a sign change of S_T in a simple lattice model. The model here proposed for $n=1$ does not agree with this rule, given that the mixed interaction is in between the interactions of the pure components for all interparticle distances.

VI. CONCLUSIONS

In this work a RNEMD study of thermodiffusion has been presented. The considered system is an equimolar mixture of two model species: they have the mass of the Ar and Kr atoms and they interact with purely repulsive potentials, which can be seen as obtained from the LJ potential for the Ar/Kr mixture by neglecting the attractive part and modifying the exponent n ($n=1, 3, 6, 9, 12$). The simulations have been conducted at different mean temperatures, in order to study the dependence of S_T on both the interaction potential and the temperature. With respect to other published works, the strategy here proposed for the extraction of S_T from the RNEMD simulation data does not require for the composition profile to be linear, while keeping the constraint for the temperature to have a linear profile. Moreover the analytical expression for the composition profile at the steady state is reported for some expressions of the dependence of S_T on the temperature.

The results obtained in this work confirm that the nature of the particle interaction strongly influences the value and the sign of S_T . In particular with medium and short range interactions ($n \geq 3$) the system behaves in agreement with the dilute gas rule, that is S_T is positive (the heavier species accumulate in the cold region) and shows a decrease with T closely following the $1/T$ behavior. In the case of long range, pseudocoulombian, interaction ($n=1$), a sign change of S_T is observed if T is changed. In particular, S_T is large and positive at small T , it decreases rapidly by increasing T and becomes negative (with the absolute value remaining quite low), then it remains almost constant and negative slowly approaching zero if T increases.

This result is in agreement with other experimental and theoretical findings which have reported that in presence of strong interactions (e.g., electrostatic in charged particles) or

specific interactions (e.g., hydrogen-bond in water/ethanol solution, etc.) S_T shows unusual behaviors when the composition or the temperature are varied and sign changes are often observed. In the present work, however, the interactions are purely repulsive, so the situation is strongly different from the case of molecular mixtures with hydrogen bonds, while the comparison with charge particles is more grounded.

An analytical expression of S_T as a function of T has been given for all interaction potentials by fitting the results of the simulations. This expression has been used in the equation defining the concentration profile at the steady state (obtained by the integration of the steady state equation of the mass flux). The concentration profile thus computed agrees with the NEMD simulation data even in the most pathological situations, as, for instance, in the cases where S_T changes of sign in the temperature range spanned by the simulation. In such simulations the concentration shows a strongly nonlinear profile (even if T is linear) and the close agreement between the analytical expression of the concentration and the simulation data validate the approach here developed.

ACKNOWLEDGMENTS

This work has been carried out with the financial support of the “Regione Autonoma della Sardegna” and of the University of Ferrara.

- ¹C. Ludwig, Sitzungsber. Preuss. Akad. Wiss., Phys. Math. Kl. **20**, 539 (1856).
- ²C. Soret, Arch. Genet. (Zur.) **3**, 48 (1879).
- ³L. Kincaid and B. Hafskold, Mol. Phys. **82**, 1099 (1994).
- ⁴S. Wiegand, J. Phys.: Condens. Matter **16**, R357 (2004).
- ⁵J. Giddings, K. Caldwell, and M. Myers, Macromolecules **9**, 106 (1976).
- ⁶P. Costesque, D. Fargue, and P. Jamet, in *Thermal Nonequilibrium Phenomena in Fluid Mixtures*, edited by W. Köhler and S. Wiegand (Springer, Berlin, 2000), p. 389.
- ⁷J. Janek and H. Timm, J. Nucl. Mater. **255**, 116 (1998).
- ⁸R. M. Fristrom and L. Monchuck, Combust. Flame **71**, 89 (1988).
- ⁹A. Ern and V. Giovangigli, Combust. Theory Modell. **2**, 349 (1998).
- ¹⁰S. Fayolle, T. Bickel, S. Le Boiteux, and A. Würger, Phys. Rev. Lett. **95**, 208301 (2005).
- ¹¹J. K. G. Dhont, J. Chem. Phys. **120**, 1632 (2004).
- ¹²Th. Völker, E. Blums, and S. Odenbach, Int. J. Heat Mass Transfer **47**, 4315 (2004).
- ¹³L. Pasti, S. Agnolet, and F. Dondi, Anal. Chem. **79**, 5284 (2007).
- ¹⁴C. Angeli and E. Leonardi, Int. J. Heat Mass Transfer **48**, 4633 (2005).
- ¹⁵S. Duhr, S. Arduini, and D. Braun, Eur. Phys. J. E **15**, 277 (2004).
- ¹⁶S. Braun and A. Libchaber, Phys. Biol. **1**, 1 (2004).
- ¹⁷S. Braun, Mod. Phys. Lett. **18**, 115 (2004).
- ¹⁸K. Clusius and G. Dickel, Naturwissenschaften **26**, 546 (1938).
- ¹⁹O. Ecenarro, J. Madariaga, J. Navarro, C. Santamaria, J. Carrion, and J. Saviron, J. Phys.: Condens. Matter **2**, 2289 (1990).
- ²⁰M. Bou-Ali, O. Ecenarro, J. Madariaga, C. Santamaria, and J. Valencia, J. Phys.: Condens. Matter **10**, 3321 (1998).
- ²¹M. Giglio and A. Vendramini, Phys. Rev. Lett. **34**, 561 (1975).
- ²²W. Köhler and P. Rossmanith, J. Phys. Chem. **99**, 5838 (1995).
- ²³H. Ning and S. Wiegand, J. Chem. Phys. **125**, 221102 (2006).
- ²⁴D. Reith and F. Müller-Plathe, J. Chem. Phys. **112**, 2436 (2000).
- ²⁵J. Bert and J. Dupuy-Philon, J. Phys.: Condens. Matter **9**, 11045 (1997).
- ²⁶J. Colombani and J. Bert, J. Chim. Phys. **96**, 1074 (1999).
- ²⁷S. Chapman and T. G. Cowling, *The Mathematical Theory of Non-Uniform Gases* (Cambridge University Press, Cambridge, 1970).
- ²⁸F. R. W. McCourt, Mol. Phys. **101**, 2181 (2003).
- ²⁹M. Lopez de Haro, E. G. D. Cohen, and J. M. Kincaid, J. Chem. Phys. **78**, 2746 (1983).

- ³⁰J. M. Kincaid, M. Lopez de Haro, and E. G. D. Cohen, *J. Chem. Phys.* **79**, 4509 (1983).
- ³¹M. Lopez de Haro and E. G. D. Cohen, *J. Chem. Phys.* **80**, 408 (1984).
- ³²J. M. Kincaid, E. G. D. Cohen, and M. Lopez de Haro, *J. Chem. Phys.* **86**, 963 (1987).
- ³³J. R. Bielenberg and H. Brenner, *Physica A* **356**, 279 (2005).
- ³⁴H. Brenner, *Phys. Rev. E* **74**, 036306 (2006).
- ³⁵C. Nieto-Draghi, J. B. Avalos, and B. Rousseau, *J. Chem. Phys.* **122**, 114503 (2005).
- ³⁶D. MacGowan and D. Evans, *Phys. Rev. A* **34**, 2133 (1986).
- ³⁷R. Vogelsang, C. Hoheisel, G. Paolini, and G. Ciccotti, *Phys. Rev. A* **36**, 3964 (1987).
- ³⁸B. Hafskjold, T. Ikeshoji, and S. K. Ratkje, *Mol. Phys.* **80**, 1389 (1993).
- ³⁹F. Müller-Plathe, *J. Chem. Phys.* **106**, 6082 (1997).
- ⁴⁰H. Schaink, H. Luo, and C. Hoheisel, *J. Chem. Phys.* **99**, 9912 (1993).
- ⁴¹J. Simon, D. Dysthe, A. H. Fuchs, and B. Rousseau, *Fluid Phase Equilib.* **150**, 151 (1998).
- ⁴²A. Perronace, G. Ciccotti, F. Leroy, A. H. Fuchs, and B. Rousseau, *Phys. Rev. E* **66**, 031201 (2002).
- ⁴³A. Perronace, C. Leppla, F. Leroy, B. Rousseau, and S. Wiegand, *J. Chem. Phys.* **116**, 3718 (2002).
- ⁴⁴P. Polyakov, M. Zhang, F. Müller-Plathe, and S. Wiegand, *J. Chem. Phys.* **127**, 014502 (2007).
- ⁴⁵C. Nieto-Draghi and J. B. Avalos, *Mol. Phys.* **101**, 2303 (2003).
- ⁴⁶P. Bordat, D. Reith, and F. Müller-Plathe, *J. Chem. Phys.* **115**, 8978 (2001).
- ⁴⁷A. Maghari and S. Yeganegi, *J. Phys. Soc. Jpn.* **69**, 1389 (2000).
- ⁴⁸A. P. Lyubartsev and A. Laaksonen, *Comput. Phys. Commun.* **128**, 565 (2000).
- ⁴⁹D. MacGowan and D. J. Evans, *Phys. Rev. A* **34**, 2133 (1986).
- ⁵⁰G. Paolini and G. Ciccotti, *Phys. Rev. A* **35**, 5156 (1987).
- ⁵¹D. M. Heyes and A. C. Brañka, *J. Chem. Phys.* **122**, 234504 (2005).
- ⁵²S. R. de Groot and P. Mazur, *Non-Equilibrium Thermodynamics* (North-Holland, Amsterdam, 1962).
- ⁵³S. Iacopini, R. Rusconi, and R. Piazza, *Eur. Phys. J. E* **19**, 59 (2006).
- ⁵⁴J. Luettmer-Strathmann, *J. Chem. Phys.* **119**, 2892 (2003).
- ⁵⁵R. Kita, S. Wiegand, and J. Luettmer-Strathmann, *J. Chem. Phys.* **121**, 3874 (2004).
- ⁵⁶S. Pan, M. Z. Saghir, M. Kawaji, C. G. Jiang, and Y. Yan, *J. Chem. Phys.* **126**, 014502 (2007).
- ⁵⁷H. Ning, R. Kita, H. Kriegs, J. Luettmer-Strathmann, and S. Wiegand, *J. Phys. Chem. B* **110**, 10746 (2006).
- ⁵⁸M. Giglio and A. Vendramini, *Phys. Rev. Lett.* **38**, 26 (1977).
- ⁵⁹B.-J. de Gans, R. Kita, B. Müller, and S. Wiegand, *J. Chem. Phys.* **118**, 8073 (2003).
- ⁶⁰B.-J. de Gans, R. Kita, S. Wiegand, and J. Luettmer-Strathmann, *Phys. Rev. Lett.* **91**, 245501 (2003).
- ⁶¹L. J. Tichacek, W. S. Kmak, and H. G. Drickamer, *J. Phys. Chem.* **60**, 660 (1956).
- ⁶²C. Debuschewitz and W. Köler, *Phys. Rev. Lett.* **87**, 055901 (2001).
- ⁶³R. Piazza and A. Guarino, *Phys. Rev. Lett.* **88**, 208302 (2002).
- ⁶⁴R. Piazza, *Philos. Mag.* **83**, 2067 (2003).
- ⁶⁵S. Iacopini and R. Piazza, *Europhys. Lett.* **63**, 247 (2003).
- ⁶⁶M. Zhang and F. Müller-Plathe, *J. Chem. Phys.* **123**, 124502 (2005).
- ⁶⁷H. Ning, J. Buitenhuis, J. K. G. Dhont, and S. Wiegand, *J. Chem. Phys.* **125**, 204911 (2006).
- ⁶⁸R. Kita, G. Kircher, and S. Wiegand, *J. Chem. Phys.* **121**, 9140 (2004).
- ⁶⁹R. Sugaya, B. A. Wolf, and R. Kita, *Biomacromolecules* **7**, 435 (2006).
- ⁷⁰S. Yeganegi and M. Zolfaghari, *Fluid Phase Equilib.* **243**, 161 (2006).
- ⁷¹C. E. Nieto-Draghi, Ph.D. thesis, Universitat Rovira i Vigili, 2003.